J. COMBIN. MATH. COMBIN. COMPUT. 127a (2025) 541–560

Journal of Combinatorial Mathematics and Combinatorial Computing
www.combinatorialpress.com/jcmcc

Combinatorial Press

Numerical resolution of nonlinear optical phenomena in solid state physics by FEM modelling

Zhiwei He[1,] ✉

[1] Basic Teaching Department, Shangqiu Institute of Technology, Shangqiu, Henan, 476000, China

ABSTRACT

When a laser beam passes through a solid physical material with a nonlinear refractive index, it can produce an optical nonlinear effect, which depends on the refractive index that changes with the light intensity. Based on an analysis of the linear principle of nonlinear optics, the article describes the coupled wave equations under the nonlinear optical phenomenon. It introduces the phase-matching method of frequency conversion and the theoretical basis of optical waveguide. Starting from the classical Maxwell's equations, the nonlinear optical transmission equations and the optical effect model are established, and then the finite element method (FEM) simulation model is constructed based on the FEM model to analyze the nonlinear optical phenomena of solid-state physical silicon materials. To verify the validity of the FEM model, the optical bistability effect and four-wave mixing spectrum of the nonlinear optical phenomena are simulated and analyzed, and the homochiral spinning effect and transmission spectrum are investigated. When the solid-state physical silicon material is rotating, the laser power required to observe the optical bistability is up to 9.51 W when the rotation rate is increased from 12 kHz to 24 kHz, and the four-wave mixing intensity decreases from 0.115 to about 0.028 when the oscillator frequency of the solid-state physical silicon material is increased from 15 MHz to 30 MHz. The plasma resonance absorption wavelength of the solid physical silicon material is at 791 nm, and the effective refractive index obtained from the simulation is 0.61 in the real part, which is only 1.64% lower than the actual refractive index. The trend of nonlinear optical phenomena in solid-state physics can be effectively obtained by using the FEM model, which provides a new idea for the application expansion of the optical force system.

Keywords: nonlinear optics; phase matching; transport equation; optical effect model; FEM model

1. Introduction

Nonlinear optics (NLO) is a new field of modern optics, which is the science of studying the nonlinear relationship between the response of a substance under the action of an intense light and the field strength presented by these optical effects are called nonlinear optical effects [1-3]. Applications of nonlinear optics

✉ Corresponding author.
E-mail address: 13500013005@sqgxy.edu.cn (Z. He).
Received 01 April 2024; Revised 30 June 2024; Accepted 15 August 2024; Published Online 15 April 2025.
DOI: 10.61091/jcmcc127a-032

include the use of nonlinear optical methods to realize the control of laser frequency, intensity (amplitude), phase, waveform, direction, polarization and other parameters. And obtaining information about the composition, structure, and properties of various substances [4-7]. In scientific research, nonlinear optical methods have made important contributions to the study of surface, interface, low-dimensional, nano, cluster, quantum confinement and other material structures, the nonlinear mechanisms of crystals, photonic crystals, semiconductors, liquid crystals, organic polymers, biological materials, as well as in the field of researching chiral matter, leptokurtic matter, negative refractive index matter and extreme physical phenomena [8-11].

At present, the research of nonlinear optics mainly focuses on two aspects: one is to open up new theories, investigate the mechanism of nonlinear optical effects, and provide theoretical basis for the design and manufacture of new nonlinear optical materials with excellent properties [12-14]. The second is the preparation and application of new and excellent nonlinear optical materials, in which a number of materials have been put into practical applications [15-16]. However, the contradiction between band redshift and nonlinear optical coefficients makes the further optimization of nonlinear optical materials encounter great difficulties, and the solution of this problem will inevitably greatly promote the optimization of the preparation and practical application of NLO materials, and thus also become a focal point of the discipline of nonlinear optics that needs to be urgently resolved [17-20].

To meet application development needs, it is also very important to seek new nonlinear optical materials based on solid-state physical materials and explore new nonlinear optical effects. This paper first sorts out the relevant theoretical foundations of nonlinear optical phenomena, including the basic principles of nonlinear optics, coupled wave equations, the phase matching method of frequency conversion, and waveguide theory. The nonlinear optical transmission equation is established based on Maxwell's equations. The nonlinear optical effect model is constructed based on this, and the nonlinear optical effect model is simulated numerically to solve the model construction by the FEM model. Finally, the numerical analysis is carried out for the nonlinear optical phenomena of solid-state physical silicon materials, including optical bistability effects, four-wave mixing spectra, homochiral spinning effects, and transmission spectral changes.

2. Nonlinear optical phenomena and waveguide theory and technology

Nonlinear optics is mainly studied in the process of laser interaction with matter, a variety of nonlinear optical effects, and the object of its research, including the laser, to change the nature and structure of matter. It also includes changing the material on the laser counter-control to realize the "light control light," mainly with the pump light to change the transmission medium to realize the signal light's control. The research object of nonlinear optics is from the original static medium to the dynamic medium, with the previous main focus on the strong light nonlinear to the weak light nonlinear research.

2.1. *Theoretical foundations of nonlinear optical phenomena*

2.1.1. Principles of nonlinear optics. Nonlinear optics (NLO) is a discipline that studies the interaction of intense light with matter, and as such, this discipline has developed gradually since the introduction of lasers [21]. Normally, all matter interacting with intense light undergoes nonlinear optical phenomena, except that some matter undergoes the phenomenon at a higher light intensity threshold, and the intensity of the nonlinear optical effect is weaker and less pronounced. Any nonlinear optical process can be split into two parts, i.e., the strong light changes the optical properties of the substance, and this change affects the properties of the light beam, i.e., the light and the substance change each other's properties.

Nonlinear optical effects originate in the nonlinear polarization of materials. The ability to move charges in a substance under the action of an electromagnetic field is called the rate of polarization. In linear optics, the electrode polarization strength P and the photoelectric field E are linearly related. i.e:

$$P = \varepsilon_0 \chi E \tag{1}$$

where ε_0 denotes the vacuum dielectric constant and χ denotes the linear polarizability.

Whereas the polarization will be nonlinear when the intense light interacts with the substance, the relation is given by:

$$P = \varepsilon_0 (\chi^{(1)} E + \chi^{(2)} EE + \chi^{(3)} EEE + \cdots) \tag{2}$$

where $\chi^{(1)}$ denotes the linear polarizability, $\chi^{(2)}, \chi^{(3)}$ denotes the second- and third-order nonlinear polarizability tensor, respectively, and so on.

Only the second-order nonlinear polarizability tensor of crystals with asymmetric centers is not zero, i.e., it shows second-order nonlinear optical effects, while theoretically all substances have third-order nonlinear optical phenomena, and their third-order nonlinear polarizability tensor can be expressed as:

$$\chi^{(2)} = \mathrm{Re}(\chi^{(2)}) + i\mathrm{Im}(\chi^{(2)}) \tag{3}$$

where $Re(\chi^{(3)}), Im(\chi^{(3)})$ denotes the real and imaginary parts of the third-order nonlinear polarizability tensor, respectively.

The nonlinear refraction coefficient and nonlinear absorption coefficient of a substance are related to the real and imaginary parts of the third-order polarizability, respectively.

2.1.2. Nonlinear coupled wave equations. For nonlinear optical phenomena in solid state physics, the fluctuation equation for the general case of light passing through a nonlinear medium can be obtained from Maxwell's system of equations. To wit:

$$\nabla \times \nabla \times \vec{E} + \mu_0 \frac{\partial^2 \vec{D}}{\partial t^2} = 0 \tag{4}$$

According to the nonresonant model describing the nonlinearity of the medium, the polarization of the medium mainly originates from the nonequilibrium displacement of the particle charges in the lattice, whereas in the incident light field as the external action field source can make the electrons in the material to be displaced. Under the action of the weak light field, the electron displacement is small, and the motion of the electron can be regarded as simple harmonic motion.

The polarization strength $\vec{P}$ of the medium and the electric field strength $\vec{E}$ of the light field satisfy a proportional linear-primary relationship, viz:

$$\vec{P}(\vec{r},t) = \varepsilon_0 \chi^{(1)} \vec{E}(\vec{r},t). \tag{5}$$

ε_0 denotes the electric constant in the vacuum medium, and $\chi^{(1)}$ denotes the linear polarizability of the dielectric material. And when the external light field is strong enough, for example, when the laser is incident on the medium, the electrons produce a large displacement away from the equilibrium position under the action of the external potential field. At this point, the asymmetry of the electron potential field comes to the fore, and the higher-order polarizability term generated in the medium cannot be neglected, and the polarization intensity $\vec{P}$ writing:

$$\vec{P}(\vec{r},t) = \varepsilon_0 \chi^{(1)} \vec{E}(\vec{r},t) + \varepsilon_0 \chi^{(2)} \vec{E}^2(\vec{r},t) + \varepsilon_0 \chi^{(3)} \vec{E}^3(\vec{r},t) + \ldots = \vec{P}^{(1)} + \vec{P}^{NL}. \tag{6}$$

where $\chi^{(n)}$ is the n nd order nonlinear polarizability tensor of the medium, so that the polarization intensity in the medium is divided into two parts: the linear polarization intensity represented by $\vec{P}^{(1)}$ and the nonlinear polarization intensity represented by $\vec{P}^{NL}$. It can be seen that the nonlinear effect produced by the medium under laser action and originates from the polarization intensity in the fluctuation equation $\vec{P}$. Therefore, the potential shift vector $\vec{D}$ can be expanded as the sum of the linear and polarization terms of the electric field, viz:

$$\vec{D} = \varepsilon_0 (1 + \chi^{(1)}) \vec{E} + \vec{P}^{NL}. \tag{7}$$

Considering the presence of a nonlinear polarization term, the nonlinear fluctuation equation can be derived as:

$$\nabla^2\vec{E}-\frac{\varepsilon^{(1)}}{c^2}\frac{\partial^2\vec{E}}{\partial t^2}=\mu_0\frac{\partial^2\vec{P}^{\mathrm{NL}}}{\partial t^2}. \tag{8}$$

Here, the propagation direction of the light field is assumed to be in the z direction, and for the frequency component of wavelength λ_n, the calculation can be obtained by Fourier transform collation under the slow-variable amplitude approximation:

$$\frac{\partial\vec{E}_n}{\partial z}=\frac{i\omega_n}{2\varepsilon_0 cn}\vec{P}_n^{NL}e^{-i\Delta kz}, \tag{9}$$

where $\Delta k=k_n^{'}-k_n$ is the phase mismatch of the wave vector. Taking the second harmonic process as an example, the frequency of the fundamental frequency light E_1 is specified to be ω_1, and the frequency of the second harmonic E_2 to be ω_2. In the small-signal approximation, the depletion of the fundamental frequency light is not considered. We can obtain the coupled wave equation for the second harmonic generated by an optical field passing through a nonlinear medium as:

$$\begin{cases}\dfrac{d\vec{E}_1(z)}{dz}=0,\\ \dfrac{d\vec{E}_2(z)}{dz}=\dfrac{i\omega_2^2}{2k_2c}\chi^{(2)}\vec{E}_1^2e^{-i\Delta kz}.\end{cases} \tag{10}$$

Set the boundary conditions of the differential equation system as $E_2(0)=0$, according to the effective nonlinear coefficient $d_{eff}=\frac{\chi^{(2)}}{2}$ and the relationship between light intensity and electric field intensity $I=2n\varepsilon_0 c|E|^2$, solve the above equation can be obtained as the second harmonic light field intensity with the nonlinear process action distance change relationship. That is:

$$I_2(z)=\frac{8\omega_1^2}{n_1n_2c^3\varepsilon_0}d_{\mathrm{eff}}^2I_1^2z^2\mathrm{sinc}^2\frac{\Delta kz}{2}. \tag{11}$$

Also, the second harmonic conversion efficiency η can be obtained as:

$$\eta=\frac{I_2}{I_1}=\frac{8\omega_1^2}{n_1n_2c^3\varepsilon_0}d_{\mathrm{eff}}^2I_1z^2\mathrm{sinc}^2\frac{\Delta kz}{2}. \tag{12}$$

The strength of the nonlinear effect is also related to the magnitude of the nonlinear coefficient of the medium, the larger the second-order nonlinear coefficient of the medium, the stronger the second harmonic it produces. The maximization of the material nonlinear coefficients is achieved by selecting a suitable crystal orientation direction, which in turn realizes an efficient second harmonic process.

2.2. *Phase matching and waveguide theory techniques*

2.2.1. Frequency conversion phase matching. In various nonlinear mixing processes, frequency conversion efficiency is a very important condition, and bit-phase matching is a key factor affecting frequency conversion efficiency. In nonlinear optics, the interaction between photons needs to satisfy the conservation of energy and momentum [22].

Taking nonlinear optical frequency doubling as an example, let the energy of the incident fundamental frequency photon be $\hbar\omega_1$ and the momentum be hk_1, i.e., $\frac{\hbar}{\lambda}$, and the energy of the frequency-doubling photon be $\hbar\omega_2$ and the momentum be hk_3, then the conservation of energy and momentum is manifested as $\omega_2=2\omega_1, k_2=2k_1$ The coupled wave equation of this frequency-doubling process is:

$$\frac{dA_1}{dz}=\frac{2i\omega_1^2 d_{eff}}{k_1c^2}A_2A_1^*e^{-i\Delta k} \tag{13}$$

$$\frac{dA_2}{dz}=\frac{i\omega_2^2 d_{eff}}{k_2c^2}A_1^2e^{-i\Delta kz} \tag{14}$$

where $\Delta k=2k_1-k_2, d_{s\sigma}$ is the effective nonlinear coefficient. The rigorous solution of this set of equations is more complicated, and the solution of the octave wave can be obtained by integrating the above equation with a small-signal approximation. At $z=0$, $A_2(0)=0$, then at $z=L$, it can be obtained:

$$A_2(L)=\frac{id_{eff}\omega_2^2A_1^2}{k_2c^2}\int_0^L\exp(i\Delta kz)dz=\frac{id_{eff}\omega_2^2A_1^2}{k_2c^2}\frac{e^{i\Delta kL}-1}{i\Delta k} \tag{15}$$

According to the relationship between light intensity and amplitude $I=2n\sqrt{\frac{\varepsilon_0}{\mu_0}}|A|^2$, the octave light intensity can be obtained as:

$$I_2=\frac{8d_{eff}^2\pi^2L^2I_1^2}{n_1^2n_2\lambda_1^2\varepsilon_0c}\sin c^2(\frac{\Delta kL}{2\pi}) \tag{16}$$

The function in Eq. shows that the light intensity of the second harmonic is closely related to the factor $\sin c^2(\Delta kL/2\pi)$. According to the nature of the function of $\sin c$, when $\Delta k=0$, $\sin c^2(\Delta kL/2\pi)$ takes the maximum value equal to 1, and the octave light conversion efficiency is maximized under this condition. And when the phase mismatch, with the increase of the action distance, when $\Delta kL=2\pi$ when the octave light intensity drops to 0, the energy back to the fundamental frequency light. According to the period of this change can be defined coherence length, expressed as:

$$L_{\grave{o}}=\frac{\pi}{\Delta k}=\frac{\lambda}{4(n_{2\omega}-n_\omega)} \tag{17}$$

The phase matching condition for a common line of octave and fundamental frequency light is:

$$\Delta k=2k_1-k_2=0 \tag{18}$$

From $k=\frac{\omega n}{c}$ to $n_1=n_2$, that is to say, the fundamental frequency light and octave light to achieve phase matching conditions require the refractive index of the fundamental frequency light in the crystal is equal to the refractive index of the octave light. Only this condition is satisfied, the two beams of light along the same direction of propagation distance L, due to the same refractive index and the same phase, so the two beams of light have the same phase, will occur in the phase length interference, the conversion efficiency will be the highest.

2.2.2. Theoretical Foundations of Optical Waveguides. In this paper, the theoretical analysis of nonlinear optical phenomena in solid state physics is often treated as waveguide structures, so this subsection provides a brief introduction to waveguide theory, giving an expression for the coefficients of the expansion of the waveguide modes of the electromagnetic field.

Let the waveguide be invariant along z direction, according to the propagation characteristics, the waveguide modes can be classified into propagation mode $(Im(k_m)\approx 0)$ and attenuation mode $(Im(k_m)>>0)$. According to the characteristics of its transverse electromagnetic field distribution, the waveguide modes can be classified into the bound state mode ($\Psi_{\pm m\to 0}$ is satisfied at the transverse infinity) and the unbound state mode ($\Psi_{\pm m}\to 0$ is not satisfied at the transverse infinity). Where k_m and $\Psi_{\pm m}$ are the phase shift constants and electromagnetic field distributions of the waveguide modes, and the subscript $+,-$ corresponds to the waveguide modes propagating positively and negatively along the z -

axis, respectively. For bound-state modes or unbound-state modes, both propagating and attenuating modes are possible.

All waveguide modes form a set of orthogonally complete basis functions, and so the total field $\Psi=[E,H]$ can be expanded with waveguide modes as:

$$\Psi=\sum_m a_m\Psi_m+\sum_m a_{-m}\Psi_{-m} \tag{19}$$

where $a_{\pm m}$ is the waveguide mode expansion coefficient, which reflects the completeness of the waveguide modes. Utilizing the orthogonality of the waveguide modes, the expansion coefficients of the positive and negative propagation modes can be expressed as, respectively

$$a_m=\frac{\iint_{z_0}(E\times H_{-m}-E_{-m}\times H)^* zdxdy}{\iint_{z_0}(E_m\times H_{-m}-E_{-m}\times H_m)^* zdxdy} \tag{20}$$

$$a_{-m}=\frac{\iint_{z_0}(E\times H_{m}-E_{m}\times H)^* zdxdy}{\iint_{z_0}(E_{-m}\times H_{m}-E_{m}\times H_{-m})^* zdxdy} \tag{21}$$

The above two equations provide the theoretical basis for the numerical calculations related to the main text.

3. FEM-based modeling of nonlinear optical effects

Nonlinear optical phenomena have a very wide range of applications in optical communications, all-optical data processing and storage, spectroscopy, and quantum information technology. However, usually the vast majority of materials have only a very weak nonlinear optical response, and generally require a very long action distance to achieve the desired optical nonlinear effect, thus severely limiting the miniaturization and integration of devices. Therefore, a long-standing research goal in the field of nonlinear optics is to develop materials with a huge optical nonlinear response, whose optical properties can be significantly altered by low-power optical fields.

3.1. Modeling of nonlinear optical effects

3.1.1. Nonlinear transmission equations. Due to the unique physical properties in the solid physical medium will make the nonlinear equations followed by the optical pulses transmitted therein more complex, starting from the classical Maxwell's equations, after some series of complex operations, the final nonlinear transmission equations can be expressed as follows:

$$\begin{aligned}&\frac{\partial A}{\partial z}+\beta_1\frac{\partial A}{\partial t}-i\sum_{m=2}^{\infty}\frac{i^m\beta_m}{m!}\frac{\partial^m A}{\partial t^m}=-\frac{1}{2}\alpha_l A-\frac{1}{2}\alpha_{FC}A+i\frac{2\pi}{\lambda}\Delta n_\lambda A\\&+i\gamma(1+\frac{i}{\omega_0}\frac{\partial}{\partial t})A(z,t)\int_{-\infty}^{t}R(t-t')\left|A(z,t)\right|^2dt'\end{aligned} \tag{22}$$

where the first term on the left describes the variation of the pulse slow-variation amplitude with distance, the second term represents the group delay of the pulse envelope, where β_1 is inversely related to the group velocity v_g, and the third term represents the effect of dispersion on the transmitted pulse. The first and second terms on the right hand side denote the linear and free carrier losses of the waveguide, respectively, the third term describes the free carrier dispersion effect, and the last term denotes the nonlinear variation experienced by the pulse under consideration of the nonlinear response [23]. The transformation can be done if the time coordinates are established in a reference system moving at group velocity:

$$T = t - z / v_g \tag{23}$$

With the relationship of the above equation, the nonlinear transmission equation can be changed to:

$$\begin{aligned}&\frac{\partial A}{\partial z} + i\sum_{m=2}^{\infty}\frac{i^m\beta_m}{m!}\frac{\partial^m A}{\partial T^m} = -\frac{1}{2}\alpha_i A - \frac{1}{2}\alpha_{FC}A + i\frac{2\pi}{\lambda}\Delta n_\lambda A \\ &+ i\gamma(1+\frac{i}{\omega_0}\frac{\partial}{\partial t})A(z,t)\int_{-\infty}^{t} R(t-t')\left| A(z,t)\right|^2 dt'\end{aligned} \tag{24}$$

For solid-state physical waveguides, the above equation is one of the most generalized nonlinear transmission equations, especially when the time duration of the pulse is only a few tens of femtoseconds or even shorter, and must be accurately described by the above equation. where $R(t)$ is the nonlinear response function, which can be written as:

$$R(t) = (1 - f_R)\delta(t) + f_R h_R(t) \tag{25}$$

where the first term on the right denotes the instantaneous electronic response, parameter f_R denotes the nucleon contribution to the nonlinear polarization, and $h_R(t)$ denotes the Raman response function, which can be derived from the Raman gain spectrum $g_R(\Omega)$. The Raman gain spectrum in the silicon medium exhibits a narrow Lorentzian bandwidth with a full width at half value of the spectrum of about 105 GHz, which is related to the imaginary part of the Fourier transform quantity $H_R(\Omega)$ of $h_R(t)$ as follows:

$$\mathrm{Im}(H_R(\Omega) = \frac{g_R(\Omega)\lambda}{4\pi n_2 f_R}) \tag{26}$$

where the Raman gain spectrum $g_R(\Omega)$ can be expressed as:

$$g_R(\Omega) = \frac{g_R\Gamma_R\Omega_R}{\Omega_R^2 - \Omega^2 - 2i\Gamma_R\Omega} \tag{27}$$

Here, g_R is the peak Raman gain, $\Omega_R / 2\pi = 15.6THz$ is the Raman frequency shift (520 cm^{-1}), and γ is a nonlinear parameter that can be expressed as:

$$\gamma = \frac{2\pi n_2}{\lambda A_{Aeff}} + i\frac{\beta_{TPA}}{2A_{Aeff}} \tag{28}$$

where A_{Aer} is the effective area of the mode field and is described as:

$$A_{Aef} = \frac{(\int_{-\infty}^{\infty}\int_{-\infty}^{\infty}\left|E(x,y)\right|^2 dxdy)^2}{\int_{-\infty}^{\infty}\int_{-\infty}^{\infty}\left|E(x,y)\right|^4 dxdy} \tag{29}$$

where $E(x, y)$ is the electric field distribution of the propagating mode in the waveguide.

For pulse durations of one hundred femtoseconds or more, the corresponding nonlinear transport equation can be simplified as:

$$\begin{aligned}&\frac{\partial A}{\partial z} + i\frac{1}{2}\beta_2\frac{\partial^2 A}{\partial T^2} - \frac{1}{6}\beta_3\frac{\partial^3 A}{\partial T^3} \\ &= -\frac{1}{2}\alpha_i A - \frac{1}{2}\alpha_{FC}A - \frac{1}{2}\frac{\beta_{TPA}}{A_{AG}}|A|^2 A + i\gamma_{SPM}|A|^2 A + i\frac{2\pi}{\lambda}\Delta v_\lambda A\end{aligned} \tag{30}$$

where A denotes the pulse slow-change amplitude, z is the transmission distance, β_m is the dispersion, α_l is the linear loss factor of the waveguide, β_{TPA} is the two-photon absorption coefficient, and γ_{SPM} is the nonlinear self-phase modulation parameter.

3.1.2. Nonlinear optical modeling. The nonlinear interaction of nonlinear optical effects in solid state physics can be relatively accurately described by the generalized nonlinear Schrödinger equation, which is also applicable to the supercontinuum spectrum generated by timely ultrashort pulse light. In this paper, we choose silicon material in solid state physics as the research object, and model its nonlinear optical effects by combining waveguide theory and nonlinear transmission equation.

As a semiconductor physical crystal material, the unique properties of silicon include two-photon absorption, free-carrier absorption, free-carrier dispersion, anisotropy, and discrete third-order nonlinear characteristics. Then the more complete theoretical model of pulsed light transmission in waveguide can be expressed as:

$$\frac{\partial A_j}{\partial z}=\sum_{m=0}^{\infty}\frac{i^{m+1}\beta_{jm}}{m!}\frac{\partial^m A_j}{\partial t^m}+i\beta_j^f(\omega,N_e,N_h)A_j+i(1+i\xi\frac{\partial}{\partial t})P_j^{NZ} \tag{31}$$

The relevant notation definitions are consistent with the nonlinear transport equations in Section 3.1.1.

Assuming that the produced free carriers are all photogenerated carriers, the produced free carrier concentration N_c is the same as the electron concentration (N_e) and the hole concentration (N_h), i.e., $N_e=N_h=N_c$, then there are:

$$\beta_j^f(\omega,N_e,N_h)=\beta_j^f(\omega,N_c)\approx\frac{n_0(\omega)}{n_i(\omega)}\left[\frac{\omega}{c}n_f(\omega,N_c)+\frac{i}{2}\alpha_f(\omega,N_c)\right] \tag{32}$$

It is clear from the above equation that the real part of section β_j represents the free carrier dispersion and the imaginary part represents the free carrier absorption. The physical meanings of the other parameters are n_0 represents the refractive index of silicon, n_i represents the mode refractive index, and nf represents the free carrier refractive index, which is related to the free carrier concentration N_c. Then:

$$n_f=\sigma_n(\omega)N_c=\zeta\left(\frac{\omega_r}{\omega}\right)^2 N_c \tag{33}$$

The free carrier absorption coefficient α_f has a mathematical expression similar to the free carrier refractive index. To wit:

$$\alpha_f=\sigma_a(\omega)N_c=1.45\times10^{-21}\left(\frac{\omega_r}{\omega}\right)^2 N_c \tag{34}$$

The evolution of the average free carrier concentration can be expressed as follows:

$$\frac{\partial N_c(z,t)}{\partial z}=\frac{\beta_{TPA}}{2h\nu_0}\frac{|A(z,t)|^4}{a_{eff}^2}-\frac{N_c(z,t)}{\tau_c} \tag{35}$$

where β_{TPA} is the two-photon absorption coefficient, a_{eff} is the effective area, and τ is the average lifetime of free carriers, which is affected by the combined effects of recombination, diffusion, and drift.

The third term at the right end of the theoretical model embodies the third-order nonlinear effect, where ξ is the frequency-dependent nonlinear parameter, which is expressed as:

$$\xi\equiv\frac{1}{\omega_0}+\frac{1}{\chi_e(\omega_0)}\frac{d\chi_e}{d\omega}\Big|\omega_0-\frac{1}{a_{eff}(\omega_0)}\frac{da_{eff}}{d\omega}\Big|\omega_0 \tag{36}$$

Eq. $\chi_e(\omega_0)\equiv\chi^e(-\omega_0;\omega_0,-\omega_0,\omega_0)$. In fact, parameter ξ is important only when the spectrum of the incident pulse broadens to a large extent during transmission through the solid-state physical waveguide. The third term at the right end of the theoretical model also has a nonlinear polarization parameter P_j^{NL}, which has the following expression in the time domain:

$$P_j^{N2}(z,t)=A_k(z,t)\int_{-\infty}^{+\infty}R_{jklm}^3(t-\tau)A_l^*(z,\tau)A_m(z,\tau)d\tau \tag{37}$$

where $R_{jklm}{}^3$ is the third-order nonlinear response function, which can be written in the following form:

$$\begin{aligned}R_{jklm}^3(t)=&\gamma_e(\omega_0)\delta(\tau)\left[\frac{\rho}{3}\left(\delta_{jk}\delta_{lm}+\delta_{jl}\delta_{lm}+\delta_{jm}\delta_{kl}\right)+(1-\rho)\delta_{jklm}\right]\\&+\gamma_R h_R(t)\left(\delta_{jl}\delta_{km}+\delta_{jm}\delta_{kl}-2\delta_{jklm}\right)\end{aligned} \tag{38}$$

The nonlinear parameter $\gamma_e(\omega_0)$ can be defined as:

$$\gamma_e(\omega_0)\equiv\gamma_{1111}^e(-\omega_0;\omega_0,-\omega_0,\omega_0)\equiv\gamma_0(\omega_0)+i\beta_{TPA}(\omega_0)/(2a_{eff}) \tag{39}$$

where $\gamma_0=con_2/(ca_{eff})$ is the nonlinear Kerr coefficient and the anisotropy parameter of silicon can be measured by p. The contribution of Raman scattering to the third-order nonlinear response is mainly in parameter γ_R, and $h_R(t)$ is the Raman response function.

3.2. *Finite element method simulation model construction*

3.2.1. FEM modeling fundamentals. The finite element method (FEM) is a numerical analysis method used to simulate and analyze physical systems. It is based on the variational principle and the weighted residual method, which decomposes the physical system into a finite number of interconnected and independent nodes and solves the system of equations using linear algebra.FEM transforms an infinite-dimensional space into a finite-dimensional space, discretizes the continuity problem, and uses polynomial functions to approximate the solution [24].

Therefore, FEM is very suitable for solving problems with complex geometry and boundary conditions. FEM has many advantages in simulating nonlinear optical phenomena in solid physics.It can accurately simulate and analyze the transport properties of solid physics independently of the location, number of layers, and shape of air holes in the solid physics cladding.The basic steps of FEM are as follows:

1) Establish the generalized function model. The system of Helmholtz equations in fiber optic transmission can be expressed as:

$$\nabla^2H+k^2H=0 \tag{40}$$

$$\nabla^2E+k^2E=0 \tag{41}$$

$$k=k_0\sqrt{[\varepsilon_r][\mu_r]} \tag{42}$$

where k_0 is the wave number in vacuum, $[\varepsilon_r]$ is the relative permittivity, and $[\mu_r]$ is the magnetic permeability tensor.

Fusing the above three equations gives:

$$\nabla\times([\varepsilon_r]^{-1}\nabla\times H)-k_0^2[\mu_r]H=0 \tag{43}$$

$$\nabla\times([\mu_r]^{-1}\nabla\times E)-k_0^2[\varepsilon_r]E=0 \tag{44}$$

The above two equations can be combined as:

$$\nabla\times([p]\nabla\times\Psi)-k_0^2[q]\Psi=0 \tag{45}$$

where at $\Psi=H$, $[p]=[\varepsilon_r]^{-1},[q]=[\mu_r]$; and when $\Psi=E$, $[p]=[\mu_r]^{-1},[q]=[\varepsilon_r]$ The generalized function of the Helmholtz equation can be expressed as:

$$F(\Psi)=\frac{1}{2}\iint_\Omega[[p](\nabla\times\Psi)^2-k_0^2[q]\Psi^2]d\Omega \tag{46}$$

If the light wave is considered to propagate uniformly in the axial direction in an optical fiber, then its electric field can be expressed as:

$$\Psi(x,y,z)=\Psi(x,y)e^{-i\beta z}=(\Psi_t(x,y)+\Psi_z(x,y))e^{-i\beta z} \tag{47}$$

where Ψ_t is the transverse component of the vector field and Ψ_z is the longitudinal component of the vector field.

Combining the above two equations gives:

$$F(\Psi)=\frac{1}{2}\iint_\Omega\begin{bmatrix}(p_z\nabla_t\times\Psi_t)\cdot(\nabla_t\times\Psi_t)-k_0^2(q_z\cdot\Psi_t)-k_0^2(q_{zz}\Psi_z)\cdot\Psi_z\\-(p_{zz}\cdot(\nabla_t\Psi_z+i\beta\Psi_t)\times\alpha_z)\cdot((\nabla_t\Psi_z+i\beta\Psi_t)\times\alpha_z)\end{bmatrix}d\Omega \tag{48}$$

where ∇_t is the transverse gradient operator.

$[p]$ and $[q]$ can be decomposed into the following equations:

$$[p]=\begin{pmatrix}p_\alpha & 0\\ 0 & P_\alpha\end{pmatrix}=\begin{pmatrix}p_{xx} & P_{xy} & 0\\ p_{yz} & P_{yy} & 0\\ 0 & 0 & P_{zz}\end{pmatrix} \tag{49}$$

$$[q]=\begin{pmatrix}q_\alpha & 0\\ 0 & q_{\alpha z}\end{pmatrix}=\begin{pmatrix}q_{xx} & q_{xy} & 0\\ q_{yz} & q_{yy} & 0\\ 0 & 0 & q_{zz}\end{pmatrix} \tag{50}$$

2) Discretization of the region to be solved. Discretization is the division of the original continuous region into a number of small units for numerical computation. Each unit can be represented by a simplified mathematical model. Generally speaking, the smaller the cell division, the more accurate the calculation results, but at the same time the calculation volume will increase. Therefore, the computational efficiency and accuracy requirements need to be weighed when choosing the division accuracy.

3) Selection of interpolation function. After discretization, it is necessary to use the interpolation function to approximate the solution of each small cell. The interpolation function is based on a continuous function between known data points and can be predicted beyond the data points. Commonly used interpolation functions include linear interpolation functions, quadratic interpolation functions, and higher order polynomial interpolation functions.

4) Establish a system of characteristic equations. Order $\Psi_t=i\beta\phi_t$, utilizing the interpolation function:

$$\Psi_t=\{N^e\}^T\{\Psi_t^e\}=\left[a_x\{U(x,y)\}^T+a_y\{V(x,y)\}^T\right]\{\Psi_t^e\} \tag{51}$$

$$\Psi_z=\{L^c\}^T\{\Psi_z^c\} \tag{52}$$

where $\{N^*\}$ is the vector basis interpolation function corresponding to the edges in each unit and $\{L^c\}$ is the node basis interpolation function corresponding to the nodes in the longitudinal direction.

It is obtained by discretizing $F(\Psi)$:

$$F(\Psi)=\frac{1}{2}[-\beta^{-2}\{\Psi_t\}^T[A_t]\{\Psi_t\}+\begin{Bmatrix}\Psi_t\\ \Psi_z\end{Bmatrix}^T\begin{pmatrix}B_{tt} & B_{tt}\\ B_{zt} & B_{zt}\end{pmatrix}\begin{bmatrix}\Psi_t\\ \Psi_z\end{bmatrix} \tag{53}$$

Multiply both sides of the above equation by β^2 simultaneously to obtain the generalized characteristic equation:

$$\begin{pmatrix}A_n & 0\\ 0 & 0\end{pmatrix}\begin{Bmatrix}\Psi_t\\ \Psi_z\end{Bmatrix}=\beta^2\begin{pmatrix}B_x & B_x\\ B_x & B_x\end{pmatrix}\begin{Bmatrix}\Psi_t\\ \Psi_z\end{Bmatrix} \tag{54}$$

Solving the above equation yields the eigenvalues and eigenvectors, which in turn yield the desired optical properties of the fiber.

3.2.2. Finite element method simulation models. Based on the FEM method given above, a two-dimensional single-period grating model of the silicon material is established to consider the incidence of a uniform planar TE wave, and the electric field expression in the current coordinate system can be written as:

$$\vec{E} = E(z)e^{-i(k_x x + k_y y)} \tag{55}$$

where k_x and k_y denote the number of waves in the X and Y directions, respectively, and the equation indicates that the wave vectors lie in the XY plane and that only Z directional components of the initial electric field exist. The model region is discretized and solved using the finite element method.

There are two types of boundary conditions involved in the grating model, as follows:

1) Port boundary conditions. Figure 1 is a schematic diagram of the system's light energy propagation. AB is the incoming port of the model; CD is the outgoing port of the model; the light wave is incident at a certain angle from the port, through the air and grating media layer, the field distribution changes, and then from the bottom of the CD outgoing. In this process, it is necessary to obtain the wavevector and optical field information of level 0 and ±1 for the subsequent calculation of diffraction efficiency and the simulation of the complete structure of the waveguide. In contrast, only one port is set up to release the incident wave and absorb the transmissive wave of level 0. Therefore, two further sub-ports need to be set up in AB and CD to absorb the outgoing waves at the non-zero diffraction level.

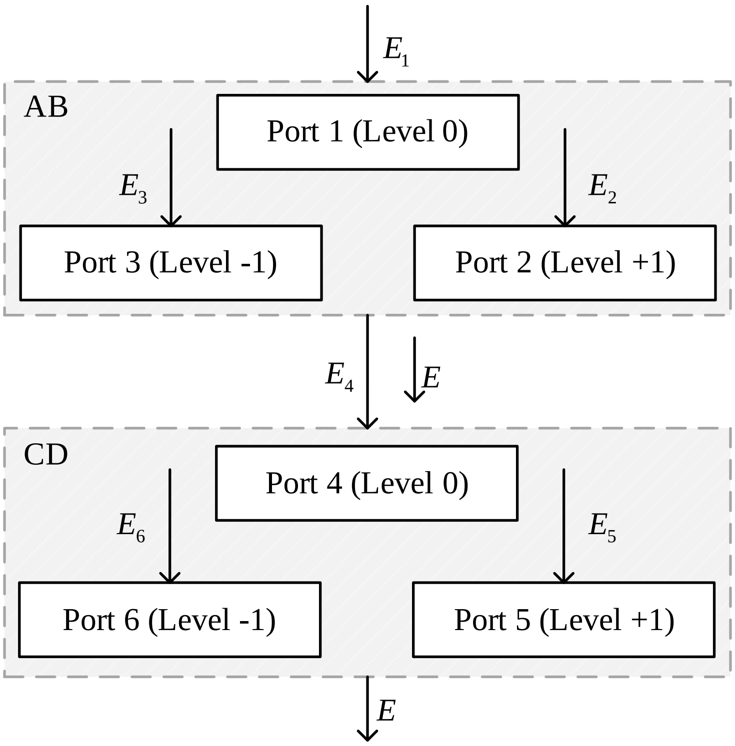

Fig. 1. Schematic diagram of light energy propagation

The component of the electric field transmitted in real time at a given location is denoted by $\vec{E}$, so the scattering parameter for port m can be expressed as the ratio of the energy transmitted through the port to the energy incident into the port. I.e:

$$S_{m1}=\begin{cases}\dfrac{\int\limits_{\partial\Omega}(\vec{E}-\vec{E}_m)\cdot\vec{E}_m}{\int\limits_{\partial\Omega}\vec{E}_m\cdot\vec{E}_m} & m=1\\ \dfrac{\int\limits_{\partial\Omega}\vec{E}\cdot\vec{E}_m}{\int\limits_{\partial\Omega}\vec{E}_m\cdot\vec{E}_m, m=2,3,4,5,6} & m=2,3,4,5,6\end{cases}\tag{56}$$

where port 1 is used to release the incident wave and therefore the corresponding component needs to be subtracted when calculating the scattering parameters.

By means of the scattering parameters, the transmittance and reflectance at all levels can be obtained by combining the respective wave vector components, i.e.:

$$Efficiency=\left|S_{m1}\cdot e^{-i\varphi}\right|^2\tag{57}$$

where denotes the phase.

2) Periodic boundary conditions. Since the grating model of the silicon material is a periodically distributed structure, the corresponding boundary conditions also exhibit periodicity along the transport direction. Floquet's theorem is a type of periodic boundary condition often used in grating solving, which describes the nature of electromagnetic field transport in periodic electromagnetic structures in the basic sense of the electric field strength of a simple harmonic electromagnetic wave $\vec{E}(x,y,z)$ The field distribution function differs by only a phase factor when moved an integer multiple of the distance of the period along the waveguide perturbation direction. In this paper, Floquet boundary conditions are used to reduce the computational effort in grating modeling, i.e:

$$\begin{cases}\vec{E}_{BC}=\vec{E}_{AD}e^{-i\vec{k}_F\cdot(\vec{r}_{BC}-\vec{r}_{AD})}\\ \vec{H}_{BC}=\vec{H}_{AD}e^{-i\vec{k}_F\cdot(\vec{r}_{BC}-\vec{r}_{AD})}\end{cases}\tag{58}$$

4. Numerical analysis of nonlinear optical phenomena in solid state physics

When the laser this high brightness light source was invented, light and material nonlinear interaction, then nonlinear optical phenomenon can be generated, it is half a century since the development of science and technology plays a very important role. Nonlinear optics between different frequencies of light waves in the energy exchange, resulting in frequency conversion of the mixing phenomenon. These optical frequency conversion effects can provide efficient, coherent light output, extend the original light source to the ultraviolet and infrared wavelength bands, and obtain broad-spectrum tunable light sources. This chapter focuses on the simulation and numerical analysis of the FEM model for the nonlinear optical phenomena of silicon materials in solid-state physics to further explore the properties of nonlinear optical phenomena in solid-state physics.

4.1. Optical bistability and four-wave mixing

4.1.1. Optical bistability effects. Before analyzing the four-wave mixing effect of silicon materials in solid materials, the following optical bistable behavior in silicon materials must be discussed. Based on the nonlinear optical model given in the previous section, the photon number and laser power in silicon materials can effectively describe the optical bistable behavior of silicon materials. To analyze the influence of different rotational directions on the optical bistable behavior of silicon materials, the variation of the average photon number with laser power for silicon materials in the case of forward rotation (Ω = 8 kHz), no rotation (Ω = 0 kHz) and backward rotation (Ω = -8 kHz) is given as shown in Fig. 2.

As can be seen from the figure, the internal photon number of silicon material for all three curves is initially in the lower stable branch; when the input laser power is gradually increased, the internal photon number firstly increases in the lower stable branch, and when it reaches the end of the lower branch, i.e., the first critical value, it jumps to the upper stable branch, i.e., the increase of the input laser power results in the increase of the internal photon number of silicon material. After coming to the upper stable branch, the number of photons inside the silicon material decreases when the input laser power decreases. However, it still varies on the upper stable branch curve. When the laser power decreases to the point where the number of photons inside the silicon material reaches a second critical value, it reaches the lower stable branch. In addition, comparing the three curves in the figure, it can be seen that the laser power required to observe optical bistability is relatively low when Ω = -8 kHz, followed by Ω = 0 kHz, and the laser power required to observe optical bistability is highest at Ω = 8 kHz, which is in the range of 9.23W to 10W. Meanwhile, at higher laser drive power, the upper stable branch of the bistability curve is larger in the case of forward rotation than in the case where the silicon material is stationary and is relatively lowest in the case of reverse rotation. Therefore, changing the rotation direction of the silicon material can effectively manipulate its optical bistable behavior, which helps better to control the nonlinear optical properties of the silicon material.

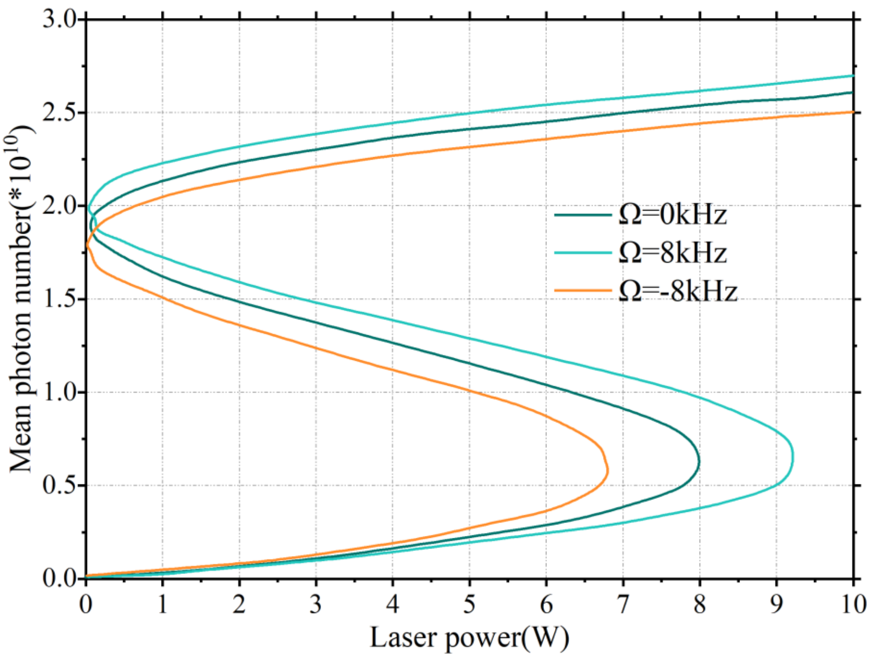

Fig. 2. Laser power change in different rotation direction

Similarly, to analyze the effect of the magnitude of the rotational rate of the silicon material on the optical bistability behavior in the silicon material, the variation of the number of photons inside the silicon material with the laser power is given for different, forward rotation rates and different reverse rotation rates. Among them, Figs. 3(a) and (b) show the laser power variation at forward and reverse rotation rates, respectively.

From Fig. 3(a), it can be seen that when the silicon material is rotated positively, the laser power required to observe the optical bistability increases from 8.48 W to 9.51 W with the increase of the rotation rate from 12 kHz to 24 kHz, which is relatively large overall. In the case of higher laser drive power, the upper stabilizing branch of the corresponding bistability curve increases as the positive rotation rate increases. In Fig. 3(b), when the counter-rotation rate of the silicon material is increased from -12 kHz to -24 kHz, the maximum laser power required for observing the optical bistability is only 7.54 W, which is relatively low, and the upper stabilizing branch of the bistable curve decreases with the increase of the counter-rotation rate. The physical nature of the above phenomenon can be explained by the fact that when a laser drives the silicon material at the same time, the radiation pressure generated inside it is resonantly coherent at the beat frequency, which induces the silicon material to vibrate at the resonance and then induces the Stokes-scattered light and the anti-Stokes-scattered light, which will re-establish a cavity field in the silicon material, inducing the generation of the optical bistability behavior.

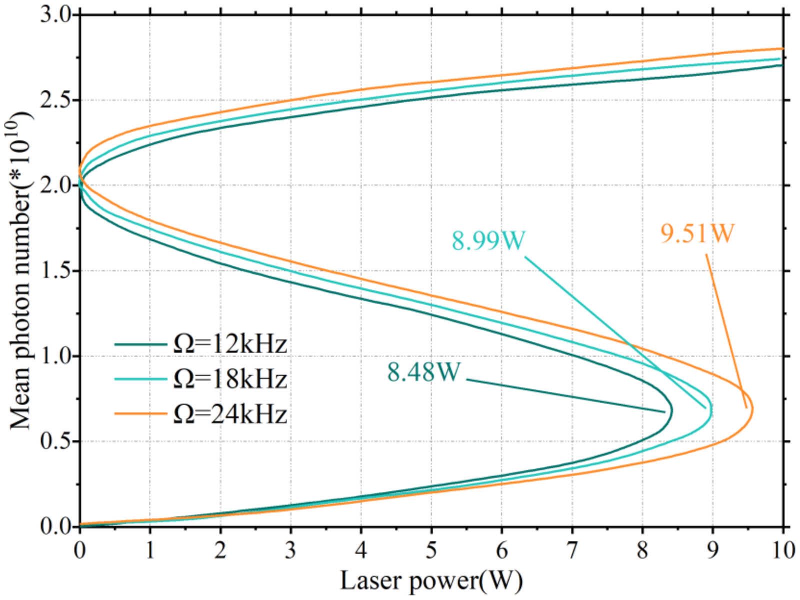

(a) Ω>0

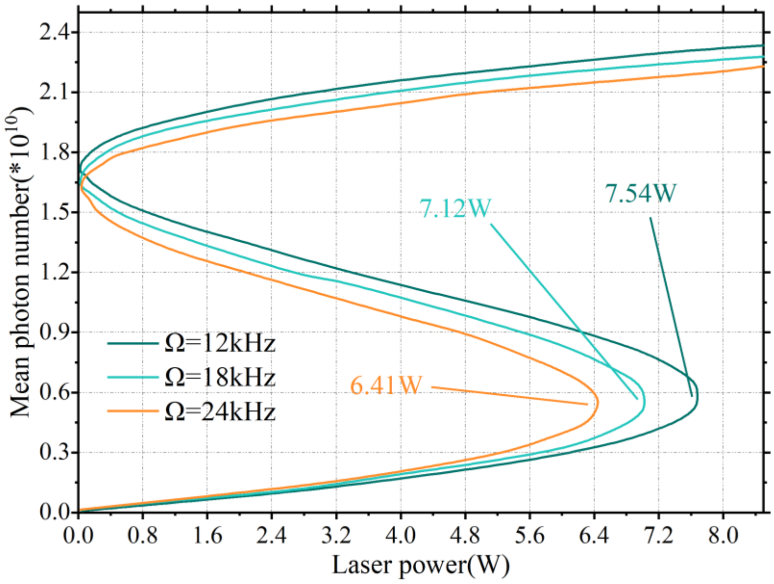

(b) Ω<0

Fig. 3. The number of photons varies with the laser power

4.1.2. Optical four-wave mixing spectrum. After clarifying the optical bistability effect of silicon materials in solid-state physics, another nonlinear behavior in solid-state physics optical force systems, i.e., the four-wave mixing phenomenon, can be further analyzed. Relying on the model of nonlinear optical effects of silicon materials established in the previous paper, the four-wave mixing intensity is calculated as a function of the change under the detector field-microwave field detuning. In this paper, we consider the four-wave mixing phenomenon under the parameters of the silicon material optical force system. The vibration frequency of silicon material is 15, 20, 25, and 30 MHz, respectively. Figure 4 shows the silicon material's nonlinear optical four-wave mixing phenomenon, where (a)~(c) are the overall change of four-wave mixing and the amplification results of the left and right spikes, respectively.

From Fig. 4(a), it is found that the four-wave mixing intensity shows a weakening trend with the increase of the silicon material vibrator frequency, i.e., the four-wave mixing intensity decreases from 0.115 to about 0.028 when the silicon material vibrator frequency is increased from 15 MHz to 30 MHz, and the position of the spikes in the four-wave mixing spectra corresponds to the detuned frequency that is closer to the silicon material vibrator frequency. The physical nature of the phenomenon comes from the quantum coherence effect generated by the interaction between the mechanical vibration mode of the silicon material and the two beams of light field through the microwave cavity. When the detected field is close to the detuned frequency between the pump field and the silicon material, the silicon material vibrator starts to vibrate and produce Stokes scattered light. During the process, the electron absorbs two photons near the detuned frequency and releases one, which induces the silicon material to produce the nonlinear optical Four-wave mixing phenomenon. At the same time, the four-wave mixing phenomenon also indicates a nonlinear optical method for measuring the frequency of the silicon material's oscillator. Determination of the frequency of the silicon material vibrator consists of two steps: the first step so that the laser field frequency and microwave field frequency are equal; the second step of the detection field scanning silicon material optical system, the four-wave mixing spectrum in the position of the spike corresponds to the vibration frequency of the silicon material vibrator. In this way, the vibration frequency of the silicon vibrator can be easily and directly measured by probing the four-wave mixing spectrum, which supports the optimization of the nonlinear optical phenomena of this solid physical material.

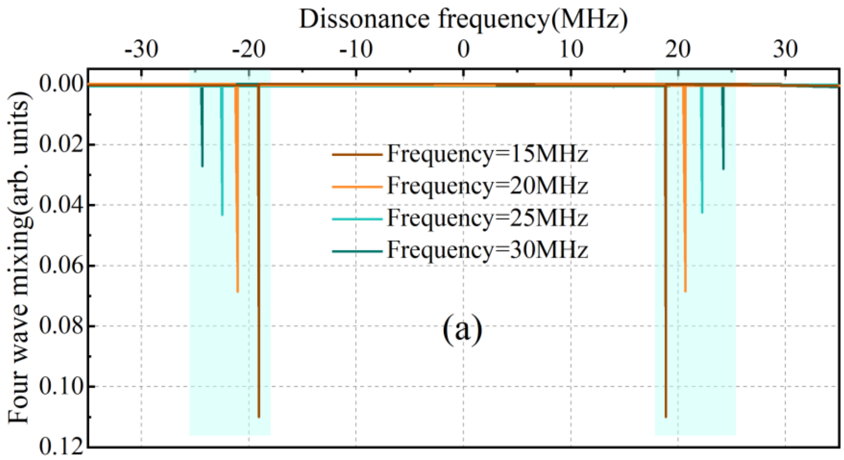

(a) Four wave mixed frequency overall change

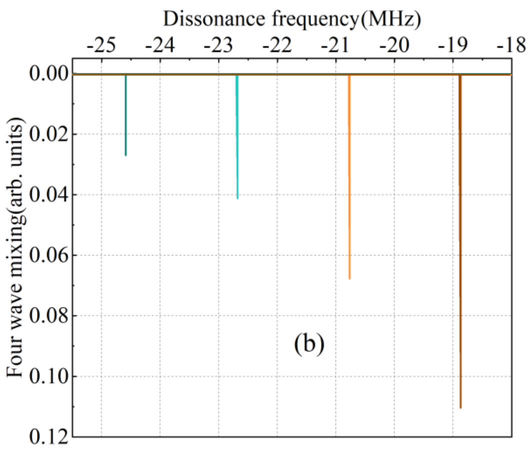

(b) Left peak

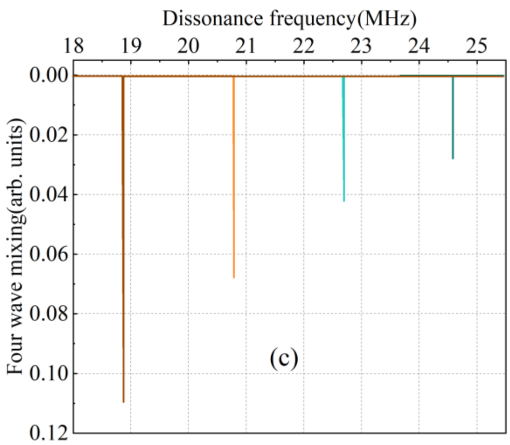

(c) Right peak

Fig. 4. Nonlinear optical four-wave mixing frequency phenomenon

4.2. *Exochiral spin effects and transmission spectra*

4.2.1. Nonlinear exochiral spin effects:

1) Effective refractive index of solid-state physical silicon materials. In classical electromagnetism theory, the interaction between an electromagnetic wave and a medium is the interaction between an electromagnetic wave and a series of scatterer combinations. Based on the nonlinear optical model of silicon material given in the previous section, numerical simulations are performed using the FEM model as a way to verify the feasibility of the FEM model in exploring the nonlinear optical linearity in solid-state physics. Fig. 5 shows the refractive index and optical resistance of silicon material and silicon crystal, where Fig. 5(a) shows the refractive index dispersion characteristics obtained from the FEM model simulation, and Fig. 5(b) shows the optical resistance dispersion characteristics of silicon material and silicon crystal itself.

The silicon crystal varies monotonically in the studied wavelength range (700∼900 nm), while the silicon material exhibits certain resonance properties. At 791 nm (noted by the vertical black dashed line in the figure), which is the plasmon resonance absorption wavelength of silicon, the real part of the effective refractive index of silicon is 0.61. The real part of the effective refractive index obtained from the simulation is only 1.64% lower compared to the effective refractive index of silicon. Using the refractive index dispersion characteristics of the silicon material obtained in this section, the numerical analysis of the effective nonlinear optical absorption coefficient of the silicon material is carried out using the FEM model.

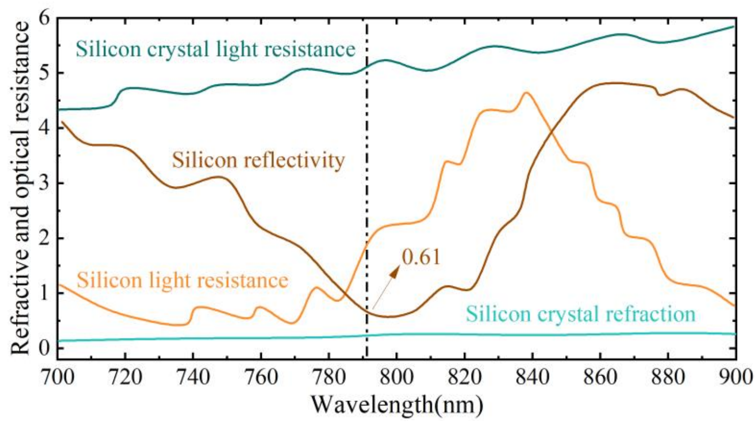

(a) Simulation result

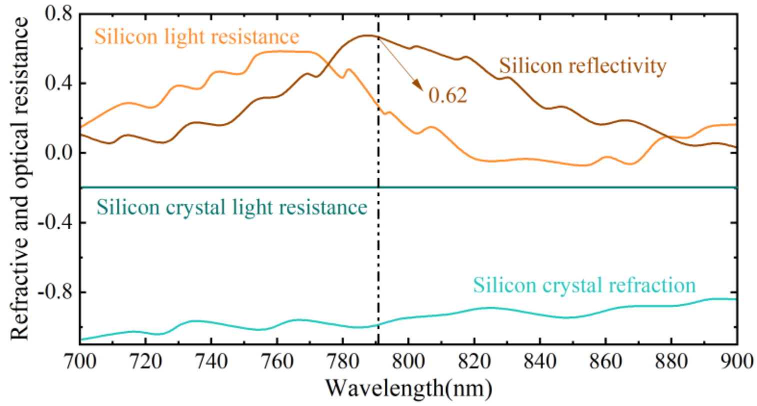

(b) Actual result

Fig. 5. Refractive index and optical resistance

2) Nonlinear exochiral rotation effect. The solid physical material chosen in this paper is silicon material, and the collection of the previous analysis of the optical bistability effect of silicon material shows that different rotational modes will destroy the optical bistability effect of the material. The reason is that the

silicon material has low symmetry, which will cause differences in the response to incident light of different polarizations and then show certain birefringence characteristics. As a result, this paper further investigates the change of solid state physical polarization state when changing the transmission of light waves. Fig. 6 shows the exochiral spinning effect of solid-state physical silicon materials, where Figs. 6(a)~(c) shows the polarization states when the y-polarized light wave is positively incident, rotated by 30 degrees, and rotated in the opposite direction, respectively.

When no rotational operation occurs in the silicon material, and the light wave is positively incident, the field distribution inside the structural unit of the silicon material (which contains the coherent superposition of the incident field and the scattered field) is shown in Fig. 6(a). The color indicates the distribution of the electric field intensity. The electromagnetic energy is mainly concentrated at the end of the C-shaped slit structure and its corners, which enhances the interaction of the electromagnetic field with the silicon atoms. The transient direction of the electric field is given by the red arrow, which shows that the electric field is symmetrically distributed about the y-direction, and the component of the combined electric field in the x-direction is canceled out after passing through the silicon material, i.e., the polarization remains in the y-direction. The yellow and orange arrows in the figure show the total electric dipole moment D and magnetic dipole moment M of a single structural unit, and the length of the arrows indicates their strengths. D is orthogonal to M under positive incidence when the silicon material will not change the polarization state of the electromagnetic wave. After rotating the silicon material around the y-axis by 30°, the distribution of the electric field will be asymmetric under the action of the external field, as shown in Fig. 6(b). The component of the combined electric field in the x-direction can not be canceled out, and the polarization state of the transmitted wave will be changed. Its total electric dipole moment D and magnetic dipole moment M are no longer orthogonal; at this time, the magnetic dipole moment in the direction of the electric dipole moment projection is no longer 0, and are elliptically polarized, at this time, there will be a spinning effect, the plane of polarization of the outgoing light will be rotated, and at the same time, the outgoing wave is elliptically polarized. When the silicon material rotates in the opposite direction, the polarization plane will rotate in the opposite direction.

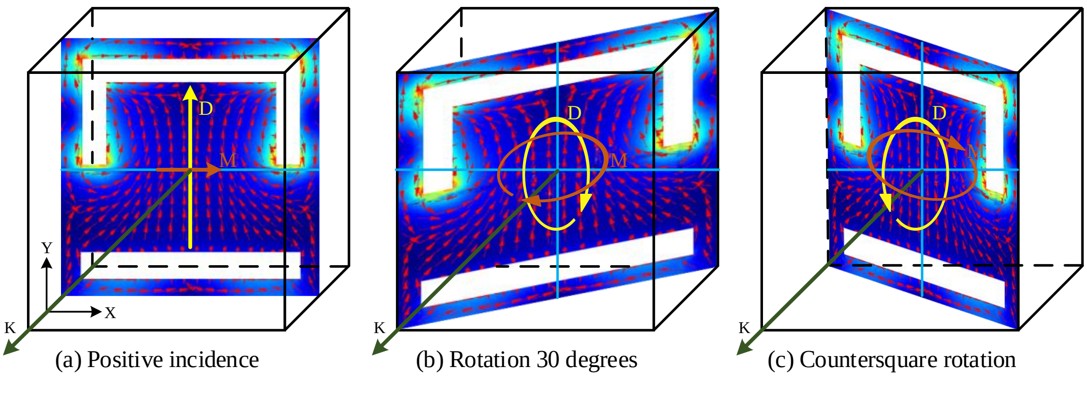

Fig. 6. The external chiral optical effect of silicon material

4.2.2. Transmission spectra of solid physical materials. A narrow linewidth tunable laser was used to sweep the wavelength range from 1500 to 1560 nm to further understand the nonlinear optical phenomena of solid-state physical silicon materials at different laser wavelengths. The projected spectra of the silicon material obtained by FEM modeling are shown in Fig. 7, where Figs. 7(a)~(c) shows the transmission spectrum, the internal resonance peaks, and the external waveguide slot resonance peaks, respectively.

Due to the small size and relatively sparse mode density, each mode in the experimental data can be well confirmed based on the simulation results. The correctness of the identification of nonlinear optical phenomena can be further increased by switching the polarization of the input light to distinguish TE/TM modes in the experiment. Each simulated mode is labeled in the figure, with the fundamental frequency mode indicated by the pink line, the higher-order transmission spectrum by the violet and brown lines, and the external waveguide slots by the blue arrows. The measured spectra match the theoretical predictions well, indicating that the external waveguide slots of the silicon material have indeed been excited. Overall, the Q-factor of the internal resonance peak is around 1.14 × 104, as determined by Floquet curve fitting, corresponding to an azimuthal mode number at a wavelength of 1543.7 nm. From the analysis, we can finally determine that the external waveguide slot is excited, as shown by the arrow in Fig. 7(a). The Q factor of the resonant peak is roughly 1.11 × 104, as shown in Fig. 7(c), corresponding to the azimuthal mode number waveguide slot mode at 1521.4 nm. This is two orders of magnitude higher than the plasma resonance peak and several times higher than the silicon vertical waveguide slot ring resonator and the horizontal air slot silicon nitride microdisk. Solid-state physics has a significant variability of nonlinear optical phenomena at different resonance peaks. When the external waveguide slots are excited, it helps to clarify the Q-factor variations contained in their resonance peaks to analyze the properties of different types of solid state physics materials and aid in the diverse applications of nonlinear optical phenomena in solid-state physics.

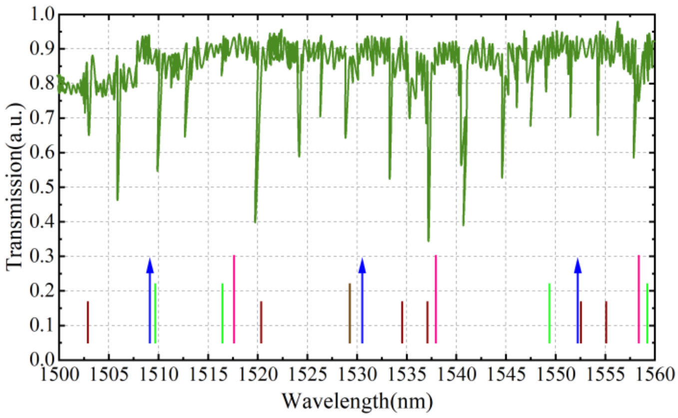

(a) Transmission spectrum

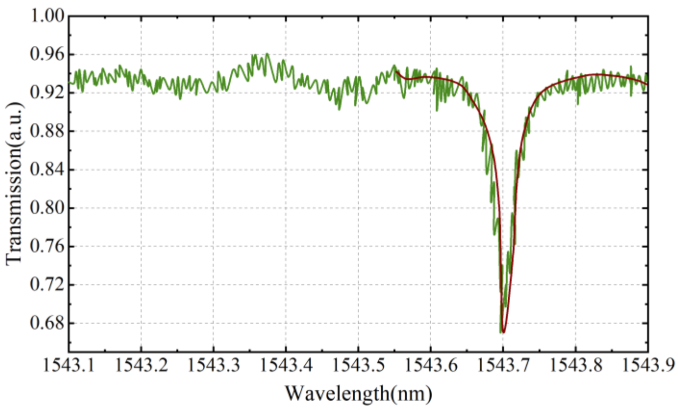

(b) Internal resonant peak

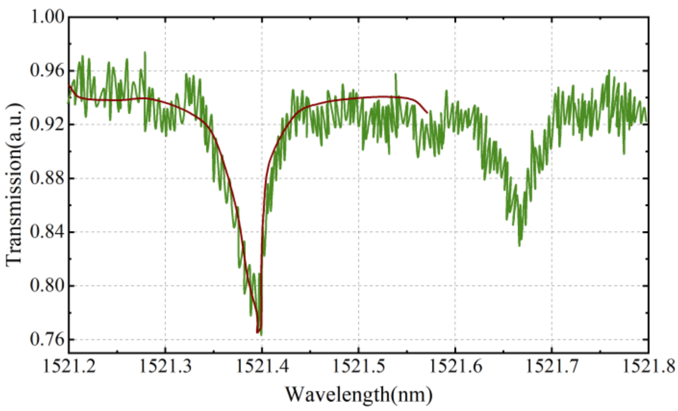

(c) External waveguide channel resonance peak

Fig. 7. The transmission spectrum of solid physical materials

5. Conclusion

In this paper, the finite element simulation model of silicon materials in solid-state physics is established by the FEN model with the linear theory of nonlinear optics as a guide, and the model is used to analyze the nonlinear optical phenomena in solid-state physics numerically.
1) The laser power required for observing optical bistability is relatively low when Ω = -8 kHz, followed by Ω = 0 kHz, while the laser power required for observing optical bistability is the highest at Ω = 8 kHz, which is in the range of 9.23 W to 10 W. The laser power required for observing optical bistability is the highest at Ω = 8 kHz, which is the highest at Ω = 8 kHz. The rotation direction of solid physical materials can be changed to manipulate their optical bistable behavior to enhance the ability to control the nonlinear optical behavior of solid physical materials.
2) When the oscillator frequency in the optical force system of the solid-state physical silicon material is increased from 15 MHz to 30 MHz, its four-wave mixing intensity decreases linearly. Its value decreases by 75.65%, and the position of the spikes in the four-wave mixing spectral line corresponds to detuning frequencies that are closer to the frequency of the oscillator of the silicon material. The detuning frequency of materials in nonlinear optics can be obtained by analyzing the four-wave mixing phenomenon in solid-state physics.
3) The effective refractive index of the solid-state physics silicon material at the plasma resonance absorption wavelength of 791 nm is 0.61, which is only 1.64% lower than that of the actual effective refractive index of the silicon material through the FEM model simulation. When changing the angle of light wave projection, there will be obvious changes in the polarization state of the solid physical material.
4) When the tunable laser is swept in the wavelength range of 1500~1560nm, corresponding to the azimuthal mode of wavelength 1543.7nm, the external waveguide groove of the solid physical material is excited. Then, there will be an obvious nonlinear optical phenomenon.

References

[1] Newell, A. (2018). Nonlinear optics. CRC Press.

[2] Powers, P. E., & Haus, J. W. (2017). Fundamentals of nonlinear optics. CRC press.

[3] Autere, A., Jussila, H., Dai, Y., Wang, Y., Lipsanen, H., & Sun, Z. (2018). Nonlinear optics with 2D layered materials. Advanced Materials, 30(24), 1705963.

[4] Krasnok, A., Tymchenko, M., & Alù, A. (2018). Nonlinear metasurfaces: a paradigm shift in nonlinear optics. Materials Today, 21(1), 8-21.

[5] Klyshko, D. N. (2018). Photons Nonlinear Optics. Routledge.

[6] Buono, W. T., & Forbes, A. (2022). Nonlinear optics with structured light. Opto-Electronic Advances, 5(6), 210174-1.

[7] Litchinitser, N. M. (2018). Nonlinear optics in metamaterials. Advances in Physics: X, 3(1), 1367628.

[8] Panoiu, N. C., Sha, W. E., Lei, D. Y., & Li, G. C. (2018). Nonlinear optics in plasmonic nanostructures. Journal of Optics, 20(8), 083001.

[9] Smith, A. V. (2018). Crystal nonlinear optics: with SNLO examples. Albuquerque, NM, USA: AS-Photonics.

[10] Perego, A. M., Turitsyn, S. K., & Staliunas, K. (2018). Gain through losses in nonlinear optics. Light: Science & Applications, 7(1), 43.

[11] Wright, L. G., Renninger, W. H., Christodoulides, D. N., & Wise, F. W. (2022). Nonlinear multimode photonics: nonlinear optics with many degrees of freedom. Optica, 9(7), 824-841.

[12] Wen, X., Gong, Z., & Li, D. (2019). Nonlinear optics of two - dimensional transition metal dichalcogenides. InfoMat, 1(3), 317-337.

[13] Hanna, M., Guichard, F., Daher, N., Bournet, Q., Délen, X., & Georges, P. (2021). Nonlinear optics in multipass cells. Laser & Photonics Reviews, 15(12), 2100220.

[14] Popov, S. V. (2017). Susceptibility tensors for nonlinear optics. Routledge.

[15] You, J. W., Bongu, S. R., Bao, Q., & Panoiu, N. C. (2018). Nonlinear optical properties and applications of 2D materials: theoretical and experimental aspects. Nanophotonics, 8(1), 63-97.

[16] Chai, X., Ropagnol, X., Raeis-Zadeh, S. M., Reid, M., Safavi-Naeini, S., & Ozaki, T. (2018). Subcycle terahertz nonlinear optics. Physical Review Letters, 121(14), 143901.

[17] Liu, X., Guo, Q., & Qiu, J. (2017). Emerging low - dimensional materials for nonlinear optics and ultrafast photonics. Advanced Materials, 29(14), 1605886.

[18] Bosshard, C. (2020). Organic nonlinear optical materials. CRC press.

[19] Zhang, Y. X., & Wang, Y. H. (2017). Nonlinear optical properties of metal nanoparticles: a review. RSC advances, 7(71), 45129-45144.

[20] Ge, F., Han, X., & Xu, J. (2021). Strongly coupled systems for nonlinear optics. Laser & Photonics Reviews, 15(4), 2000514.

[21] Renato Medeiros,Leandro R Franco,Francisco A P Osório,Clodoaldo Valverde,Marcos A Castro & Tertius L Fonseca. (2024). Understanding Nonlinear Optical Phenomena in N-Pyrimidinyl Stilbazolium Crystals via a Self-Consistent Electrostatic Embedding - DFT Approach. ACS omega(29),32080-32088.

[22] Elham Nazemosadat,Hamed Pourbeyram & Arash Mafi. (2016). Phase matching for spontaneous frequency conversion via four-wave mixing in graded-index multimode optical fibers. JOSA B(2),144-150.

[23] Sadaf Maasoomah,Akram Ghazala & Arshed Saima. (2024). Optical exact soliton solutions of nonlinear optical transmission equation using two explicit methods. Optical and Quantum Electronics(4).

[24] Mahmood Muhammad Arif,Tariq Usman,Oane Mihai & Liou Frank. (2024). Analytical and FEM models for thermal analysis and residual stresses using wire arc-based welding and additive manufacturing of SUS304. The International Journal of Advanced Manufacturing Technology(5-6),2363-2380.